SAGE-Hindawi Access to Research
International Journal of Electrochemistry
Volume 2011, Article ID 505929, 10 pages
doi:10.4061/2011/505929

Research Article

An Electrochemical Impedance Study of AISI 321 Stainless Steel in 0.5 M H_2SO_4

A. Fattah-Alhosseini, M. Mosavi, and A. Allahdadi

Faculty of Engineering, Buali Sina University, Hamedan 65178-38695, Iran

Correspondence should be addressed to A. Fattah-Alhosseini, a.fattah@basu.ac.ir

Received 2 February 2011; Revised 16 March 2011; Accepted 30 March 2011

Academic Editor: Jay D. Wadhawan

The electrochemical behavior of passive films formed on AISI 321 has been examined using electrochemical impedance spectroscopy. AISI 321 is characterized by high interfacial impedance, thereby illustrating its high corrosion resistance. Results showed that the interfacial impedance and the polarization resistance initially increase with applied potential, within the low potential. However, at a sufficiently high potential ($E > 0.6$ V), the interfacial impedance and the polarization resistance decrease with increasing potential. The impedance data were adequately represented by an equivalent electrical circuit model based on point defect model, which described the behavior of the passive film on stainless steel more satisfactorily than the proposed models.

1. Introduction

The excellent corrosion resistance of stainless steels is largely due to the protective oxide passive films formed on the surface. Many analytical studies have agreed that the passive film on stainless steels consists of Cr-enriched (Fe, Cr) oxide/hydroxide, which in many cases are no thicker than a few nanometers, act as a reactivity barrier between the stainless steel and the environment [1–3]. The electrochemical polarization method, including anodic passivation, enhances the preferential dissolution of iron into solution and the enrichment of chromium in the passive film, and hence this method is effective for increasing stability, compaction, and corrosion resistance of the passive films [4, 5]. The anodic current density of anodic films is lowered by several orders of magnitude than that of naturally grown oxide films. The chemical composition, the structure, and the thickness of electrochemically formed passive films on stainless steel change not only with environment but especially with passivation potential [6–9].

Compared with many theories qualitatively describing the passive state, the point defect model (PDM) provides a microscopic description of the growth and breakdown of a passive film and an analytical expression for the flux and the concentration of vacancies within the passive film, and hence which afford an opportunity for quantitative analysis [10, 14–18].

The PDM assumes that the transport of matter through the film takes place via ionic point defects. This model further postulates that the point defects present in a passive film are, in general, cation vacancies ($V_M^{\chi-}$), oxygen vacancies ($V_O^{\cdot\cdot}$), and cation interstitials ($M_i^{\chi+}$), as designated by the Kroger-Vink notation. The defect structure of the passive film can be understood in terms of the set of defect generation and annihilation reactions occurring at the metal/passive film interface and at the passive film/solution interface, as depicted in Figure 1 [11–13].

This transport is necessary for any growth of the film. The presence of point defects also provides a path for the cations formed from the substrate metal to pass through the film into the solution. Point defects are formed and annihilated in reactions proceeding at the metal/film and film/solution interfaces. The rates of these reactions and of the defect transport determine to a great extent the electrical and electrochemical properties of the film [11–13].

Electrochemical impedance spectroscopy (EIS) has been widely used for studying the electrochemical mechanisms occurring on the electrodes. EIS data can be used to establish an equivalent electrical circuit model for the

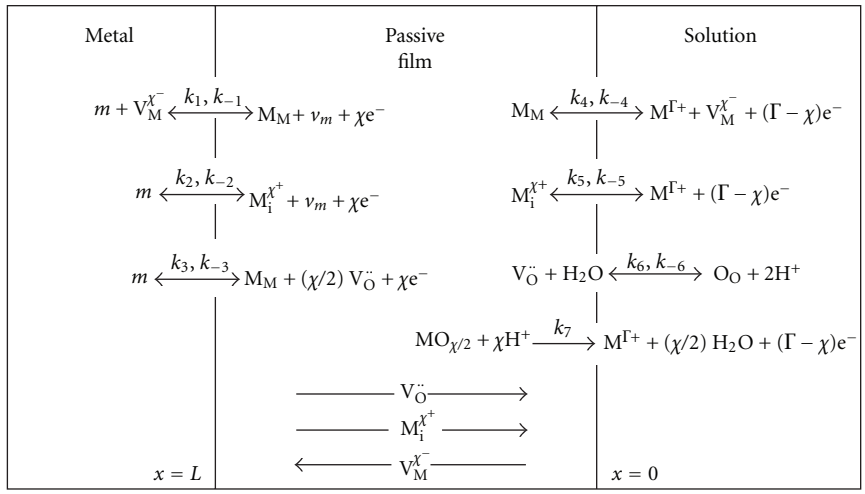

Figure 1: Interfacial defect generation-annihilation reactions that are postulated to occur in the growth of anodic barrier oxide films according to the PDM. m = metal atom, $V_M^{\chi-}$ = cation vacancy on the metal sublattice of the barrier layer, $M_i^{\chi+}$ = interstitial cation, M_M = metal cation on the metal sublattice of the barrier layer, $V_O^{\cdot\cdot}$ = oxygen vacancy on the oxygen sublattice of the barrier layer, O_O = oxygen anion on the oxygen sublattice of the barrier layer, $M^{\Gamma+}$ = metal cation in solution [10–13].

Table 1: Nominal chemical composition of AISI 321 stainless steel.

Elements	Cr	Ni	Mn	Si	C	Ti	Nb	S	Mo	Cu	**Fe**
AISI 321/wt%	19.1	9.85	1.65	0.297	0.086	0.68	0.035	0.05	0.16	0.172	Bal

electrochemical processes of electrodes. The various elements in this equivalent circuit are related to the metal/film and film/solution interfaces and the phenomena occurring inside the passive film [19, 20]. EIS measurements make it possible to obtain some information on the mechanism, establishing a theoretical transfer function, and developing the passive film growth model [21, 22].

AISI 321 stainless steel is a most popular alloy, used extensively because of its good corrosion resistance; its passive films have been the subject of many investigations. In spite of the relatively large amount of research on the electrical properties of passive films anodically formed; however, few papers have been published on a systematic study of the impedance behavior. The great complexity of the metal/passive film/electrolyte system of stainless steels makes the clarification of the passive film difficult. In this work, EIS measurements were made in a large range of frequencies in order to get more information on the passive film electrochemically grown on AISI 321 stainless steel/solution properties.

2. Experimental Procedures

Specimens were fabricated from 1 cm diameter rods of AISI 321 stainless steel; the nominal composition is given in Table 1. The samples were placed in stainless steel sacks and were annealed in inert environment (Ar gas) to eliminate the cold work effect due to cutting process. The annealing was performed at 1050°C for 90 min followed by water quenching. The pretreatment applied on specimens consisted of mechanical polishing using emery papers up to 1200 grade, degreasing and rinsing in distilled water. A three-electrode cell featuring a Pt counter electrode and a saturated calomel electrode (SCE) was employed. All the potential values in the text are relative to the SCE. The solution (0.5 M H_2SO_4) was prepared from analytical-grade 97% H_2SO_4 and distilled water. Prior to each experiment, the working electrode was catholically polarized at −1.2 V for 5 min.

Impedance investigations were performed using an EG&G Model 273A potentiostat/galvanostat controlled by a personal computer at ambient temperature (23–25°C). Passive films on AISI 321 stainless steel were formed potentiostatically at DC potentials selected based on the passive region of anodic curve for 1 h and then EIS measurements were done. Each electrochemical measurement was repeated at least three times. An excitation voltage of 10 mV (peak-to-peak) and an applied frequency ranging from 100 kHz to 10 mHz have been used. For EIS data modeling and curve-fitting method, *Z*-View2 impedance software "Equivalent Circuit" was used. This program is based on the method of nonlinear least squares, which allows nonideal electrochemical behavior to be modeled.

3. Results and Discussion

3.1. Polarization Behavior. The potentidynamic polarization curve of AISI 321 stainless steel in 0.5 M H_2SO_4 solution is shown in Figure 2. According to Figure 2, two stages of the passive process can be distinguished in the curve. The low potential passive region ranges from about −0.15 to 0.6 V

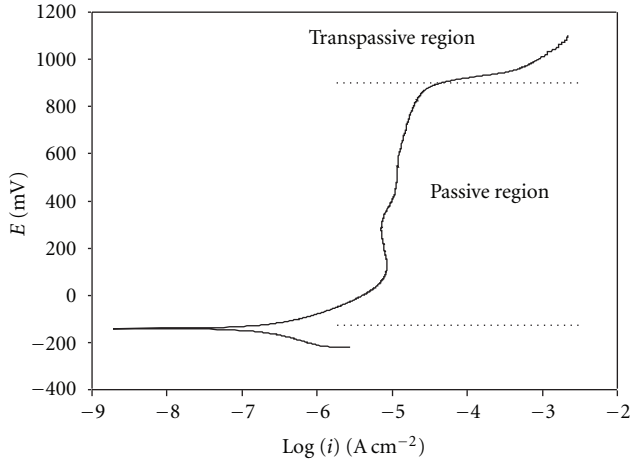

Figure 2: Potentiodynamic polarization curve for AISI 321 stainless steel in 0.5 M H_2SO_4.

(region I). In region II, the comparatively slow increase of the current in the potential range 0.6–0.9 V could be connected to the formation of high valency Cr [23] in the film prior to transpassive dissolution. The steeper increase in the range 0.9 to 1.1 V is most probably related to the onset of the transpassive dissolution.

3.2. EIS Measurements. The electrochemical behavior of the anodic passive films on AISI 321 stainless steel in 0.5 M H_2SO_4 have been evaluated by means of EIS measurements. For this purpose, passive films on stainless steel electrode were formed potentiostatically at DC potentials selected based on the passive region of anodic curve for 1 h and then EIS measurements were done.

Typical Nyquist and Bode plots for anodic oxide films are presented in Figure 3. Bode plots have been added for the representation of the impedance spectra because the magnitude of the impedance at low frequencies is several orders of magnitude higher than that at high frequencies, and thus high-frequency features are difficult to discern in a Nyquist plot. In the frequency range of measurement, all impedance spectra have the same features.

Figure 4 indicates that the impedance magnitude at low frequencies initially increase with film formation potential, within the low passive potential. However, at a sufficiently high passive potential ($E > 0.6$ V) the impedance magnitude decrease with increasing potential. The high impedance values in this low-frequency region can be associated with the presence of the barrier layer of the passive film.

3.3. The Physical and Mathematical Passivation Models. For many years, a great number of models have been put forward through the research and analysis of the EIS of different systems. Among these models, the six main ones are as follows.

Model A. The interface resistance R and the capacitance C are simply paralleled to represent the passive electrode system [24–30]. When measuring the impedance of the actual system, the obtained capacitance sometimes may deviate from the "pure capacitance." Therefore, a constant phase element (Q) is introduced for the fitting to replace capacitor C [31–33]. In Figure 5(a), R_s is the uncompensated solution resistance; R_1 and Q_1 are the interface resistance and the interface constant phase element, respectively. The mathematical expression of the impedance of the electrode system in this model is

$$Z = R_s + \frac{1}{1/R_1 + Y_0(j\omega)^n}. \quad (1)$$

The impedance of the constant phase element Q is presented by

$$Z_Q = \left[Y_0(j\omega)^n\right]^{-1}, \quad (2)$$

where n is associated with the roughness of the electrode surface and Y_0 is a frequency-independent real constant representing the total capacitance of the Q. When $n = 1$, it means that Q is equivalent to a pure capacitor and $Y_0 = C$ [34–38].

Model B. It is believed that the impedance of the passive films of metals comes from the migration of metal and oxygen vacancies within the film. According to this statement, the process of migration of metal and oxygen vacancies within the passive film has the form of a Warburg impedance. When the oxygen vacancies are dominant in the passive film, the impedance of the film is $Z_f = \sigma_0\omega^{-1/2}(1 - j)$ [39, 40]. Figure 5(b) shows the equivalent circuit of this model [41–44]; here R_1 is the charge transfer resistance. The mathematic expression of the impedance of this electrode system is

$$Z = R_s + \frac{1}{Y_0(j\omega)^n + 1/(R_1 + Z_D)}. \quad (3)$$

Model C. A constant phase element (Q_2) is used to represent the transfer of the charged particles within the passive film, shown in Figure 5(c). It is believed that the passive film has capacitive characters. Jamnik et al. [45] postulate that, in the Nyquist plot, the diffusion of the charged particles in a solid must be combined with a reaction impedance that may result in a slope greater than 45°, but not 90°. The mathematic expression of the impedance of the electrode system is

$$Z = R_s + \frac{1}{1/R_1 + Y_{01}(j\omega)^{n_1}} + \frac{1}{Y_{02}(j\omega)^{n_2}}. \quad (4)$$

Model D. Two $R//Q$ parallel circuits are used, to represent the electrochemical activities of the passive film and the film/solution interface, respectively (Figure 5(d)) [46]. In this figure, R_1 and Q_1 are the charge transfer resistance and the double layer capacitance, respectively. R_2 and Q_2 are the film resistance and the film capacitance, or the resistance and capacitance of the space charge layer, respectively. The

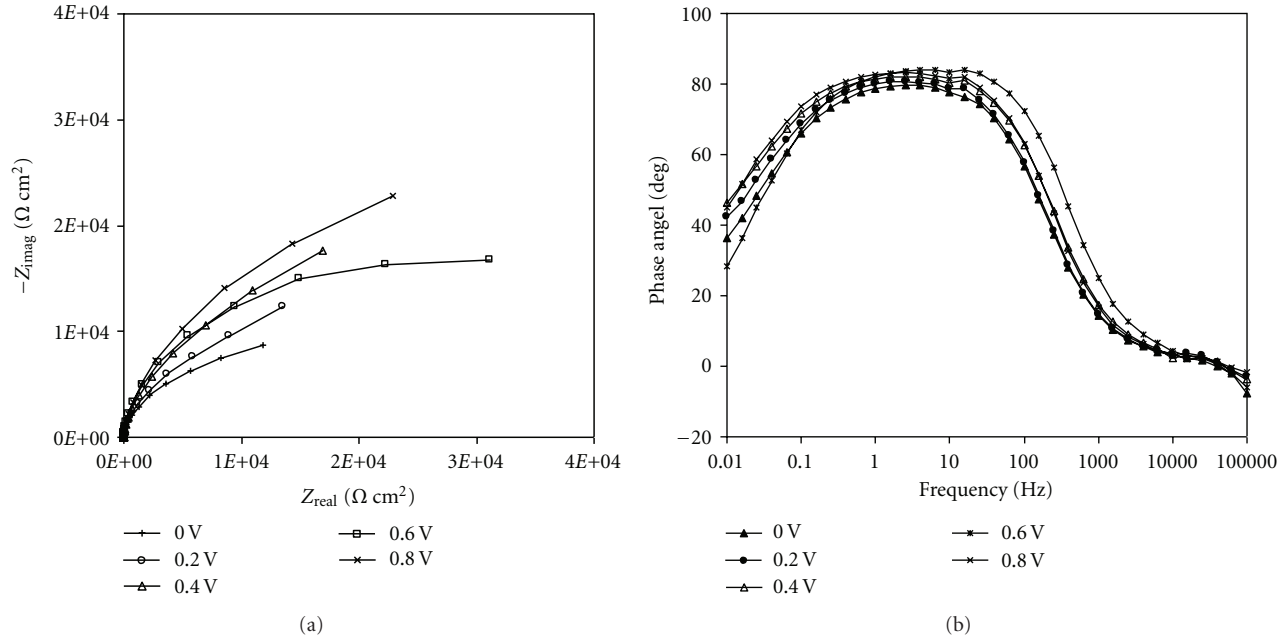

Figure 3: Impedance spectra for AISI 321 stainless steel in 0.5 M H_2SO_4 solution as a function of film formation potential: (a) Nyquist plots and (b) Bode plots.

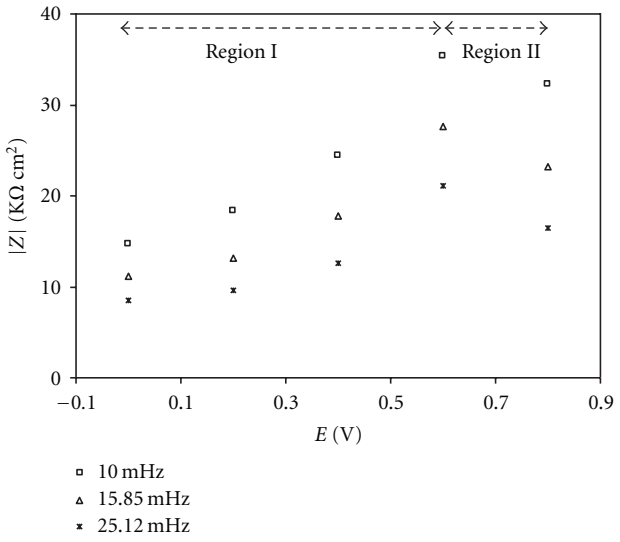

Figure 4: Effect of film formation potential on impedance magnitude of AISI 321 stainless steel in 0.5 M H_2SO_4 at low frequencies.

mathematical expression of the impedance of the electrode system in this model is

$$Z = R_s + \frac{1}{1/R_1 + Y_{01}(j\omega)^{n_1}} + \frac{1}{1/R_2 + Y_{02}(j\omega)^{n_2}}. \quad (5)$$

Model E. Figure 5(e) shows a graphical representation of the electrochemical system and the equivalent circuit [47]. C_1 and R_1 represent the capacitive and resistive contributions of the passive film/metal interface, C_P and R_P represent the bulk passive film, Q and R_2 represent the solution/passive film interface, and R_s is the uncompensated solution resistance. The mathematical expression of the impedance of the electrode system in this model is

$$Z = R_s + \frac{1}{1/R_1 + Y_{01}(j\omega)^{n_1}} + \frac{1}{1/R_P + C_P(j\omega)^{n}} + \frac{1}{1/R_2 + C_2(j\omega)^{n}}. \quad (6)$$

Model F. Figure 5(f) shows a graphical representation of the electrochemical system and the equivalent circuit [48]. The equivalent circuit is a combination of three branches, including the uncompensated solution resistance, R_s. R_{ct} and Q_{dl} are the charge-transfer resistance of the interfacial reaction and the double-layer capacitance. R_P and Q_P are related to the electronic charging in the passive oxide film. Z_D represents the impedance diffusion, which can be related to ionic defect transport through the passive film. R_1 and Q_1 indicate the contribution of surface states. According to Cahan and Chen [47], in some passivation conditions an excess proton creates a corresponding Fe^{2+} and a deficient proton causes an equivalent Fe^{3+} in the film, and these ions play the role of surface states. The mathematical expression of the impedance of the electrode system in this model is

$$Z = R_s + \frac{1}{1/R_{ct} + Y_{0dl}(j\omega)^{n_{dl}}} + \frac{1}{1/(R_P + Z_D) + Y_{0P}(j\omega)^{n_P}} + \frac{1}{1/R_1 + Y_{01}(j\omega)^{n_1}}. \quad (7)$$

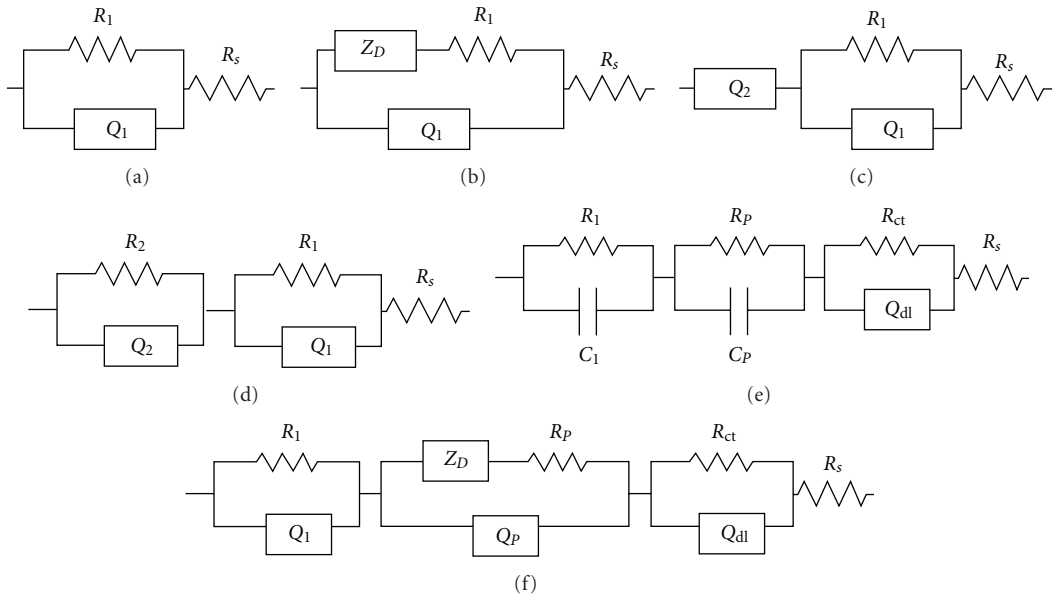

Figure 5: Physical models for metal/passive film/solution system: (a) Model A, (b) Model B, (c) Model C, (d) Model D, (e) Model E, and (f) Model F.

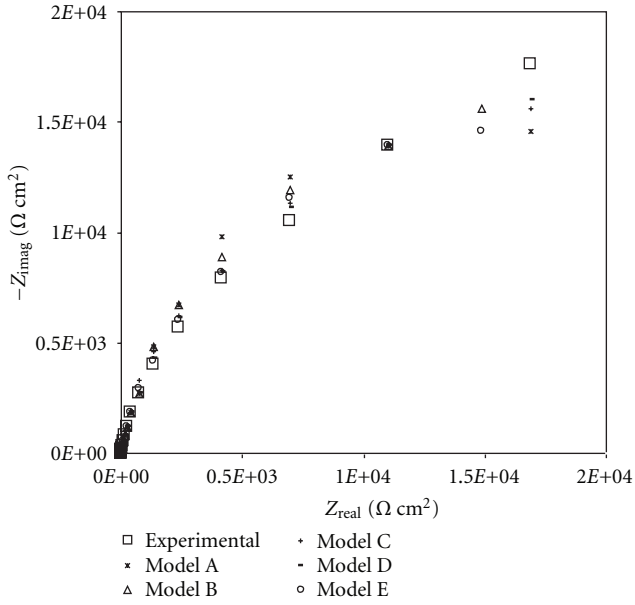

Figure 6: The fitting results of typical Nyquist plots for passive films on AISI 321 electrodes were formed potentiostatically at 0.4 V using the five models.

The impedance of diffusion is given by

$$Z_D = R_D \frac{\tanh\left(j\omega(\delta^2/D)\right)^{n'}}{\left(j\omega(\delta^2/D)\right)^{n'}}, \tag{8}$$

where R_D is the diffusion resistance, δ is the effective diffusion thickness, D is the effective diffusion coefficient, and n' is the generalized finite Warburg exponent.

According to the PDM, at the metal/passive film interface, the annihilation of metal vacancies (reaction (9)), formation of oxygen vacancies (reaction (10)) and injection of metal interstitials (reaction (11)) take place [16]:

$$\mathrm{M} + \mathrm{V}_{\mathrm{M}}^{3-} \xrightarrow{r_1} \mathrm{M}_{\mathrm{M}} + 3\mathrm{e}^- \tag{9}$$

$$\mathrm{M} \xrightarrow{r_2} \mathrm{M}_{\mathrm{M}} + \frac{3}{2}\mathrm{V}_{\mathrm{O}}^{2+} + 3\mathrm{e}^- \tag{10}$$

$$\mathrm{M} \xrightarrow{r_3} \mathrm{M}_{\mathrm{i}}^{2+} + 2\mathrm{e}^- \tag{11}$$

In the passive film, high-field assisted migration of defects is assumed to proceed. At the passive film/solution interface, metal vacancies are generated via abstraction of metal positions in the oxide lattice (reaction (12)), the interstitials are dissolved (reaction (13)) and the oxygen vacancies react with adsorbed water (reaction (14)). Reaction (14), together with reaction (10) and transport of oxygen vacancies outwards (i.e., motion of oxygen ions inwards as indicated above), result in film growth [16]:

$$\mathrm{M}_{\mathrm{M}} \xrightarrow{r_4} \mathrm{V}_{\mathrm{M}}^{3-} + \mathrm{M}_{\mathrm{aq}}^{3+} \tag{12}$$

$$\mathrm{M}_{\mathrm{i}}^{2+} \xrightarrow{r_5} \mathrm{M}_{\mathrm{aq}}^{x+} + \left(\chi - 2\right)\mathrm{e}^- \tag{13}$$

$$\frac{3}{2}\mathrm{H_2O} + \frac{3}{2}\mathrm{V}_{\mathrm{O}}^{2+} \xrightarrow{r_6} \frac{3}{2}\mathrm{O}_{\mathrm{O}} + 3\mathrm{H}^+ \tag{14}$$

In order to preserve the steady-state thickness of the film at a given potential, the growth reaction has to be balanced by chemical dissolution of the film

$$\mathrm{M_2O_3} + 6\mathrm{H}^+ \xrightarrow{r_7} 2\mathrm{M}_{\mathrm{aq}}^{3+} + 3\mathrm{H_2O} \tag{15}$$

The overall impedance of the metal/passive film/solution (Z) is defined as the sum of the interfacial impedances at the

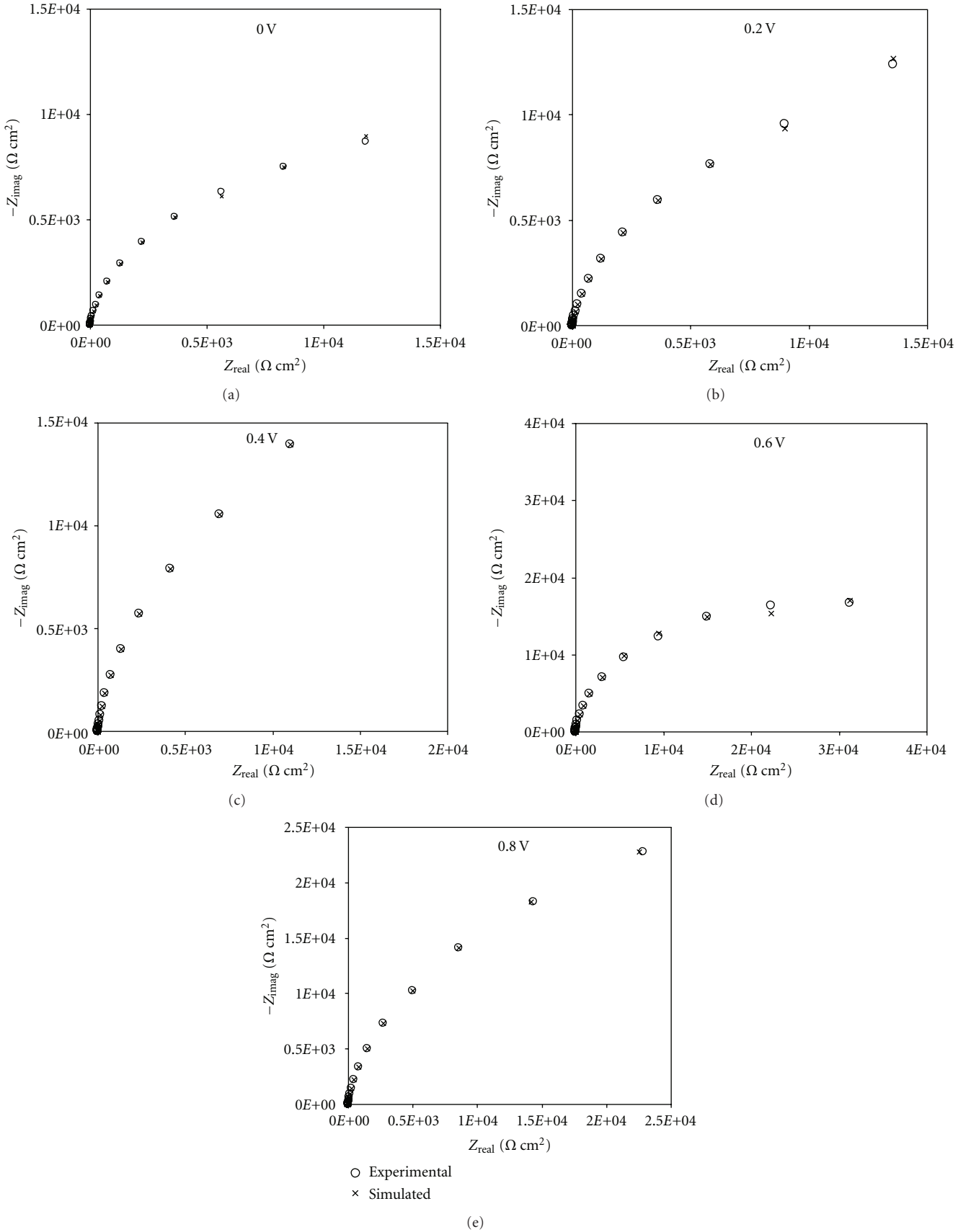

FIGURE 7: Nyquist plots for AISI 321 stainless steel in 0.5 M H_2SO_4 and as a function of potential showing a comparison between the experimental and simulated data.

Table 2: Passive element values for the equivalent circuit of Model F obtained from the fitting procedure of types.

E	R_1	Y_{01}	n_1	R_P	Y_{0P}	n_2	R_D	δ^2/D	R_{ct}	Y_{03}	n_3
V	$\Omega\,cm^2$	$\mu F\,cm^{-2}$		$k\Omega\,cm^2$	$\mu F\,cm^{-2}$		$\Omega\,cm^2$		$k\Omega\,cm^2$	$\mu F\,cm^{-2}$	
0.0	0.42	954.44	0.78	0.76	221.25	0.95	48.80	4.44	15.379	538.03	0.89
0.2	0.50	243.53	0.68	1.31	172.42	0.91	17.99	4.41	18.68	543.89	0.91
0.4	0.52	228.71	0.71	1.51	132.95	0.86	14.49	5.01	22.97	443.53	0.99
0.6	0.59	181.42	0.95	4.93	125.46	0.90	9.27	4.13	26.85	299.03	0.99
0.8	0.39	196.66	0.70	1.78	105.14	0.85	10.52	4.96	29.72	362.83	0.99

metal/passive film ($Z_{m/f}$) and passive film/solution ($Z_{f/s}$) interfaces and the transport impedance in the passive film (Z_f) [49]:

$$Z = Z_{m/f} + Z_f + Z_{f/s}. \tag{16}$$

The faradic impedances of the metal/passive film and passive film/solution interfaces have in general the form of charge transfer resistances which are functions of the rate constants and Tafel coefficients of the interfacial reactions [12, 49]:

$$\begin{aligned} Z_{m/f}^{-1} &= R_{m/f}^{-1} + j\omega C_{m/f}, \\ Z_{f/s}^{-1} &= R_{f/s}^{-1} + j\omega C_{f/s}. \end{aligned} \tag{17}$$

Assuming the transport of both ionic and electronic defects contribute to the passive film impedance, it can be shown that [50, 51]

$$Z_f^{-1} = (Z_e^{-1} + Z_{ion}^{-1}). \tag{18}$$

Where Z_e is impedance due to electron transport through the passive film and Z_{ion} is impedance due to ion transport through the passive film. Therefore it is observed clearly that the impedance data were adequately represented by an equivalent electrical circuit model (Model F) based on PDM, which described the behavior of the passive film on stainless steel more satisfactorily than the proposed models.

3.4. The Fitting Results. Figure 6 shows the fitting results of typical Nyquist plots for passive films on AISI 321 electrodes were formed potentiostatically at 0.4 V using the five models. It is found that the fitting errors of Models A, B, C, and D are relatively high. In Model A, the EIS is corresponding to a capacitive loop. When fitting the data, the fitting error increases remarkably. In Model B, diffusion process occurs at low frequency and has a form of Warburg impedance. When fitting with this model, large errors occur in the low-frequency region. Therefore, Models A and B are not suitable for this system.

In Model C, R_1 is the charge transfer resistance. Q_1 and Q_2, respectively, reflect the double-layer capacitance and the substance transfer processes in the passive film. From the physical point of view, it is not reasonable to represent the substance transfer within the passive film simply by a capacitor. Model D consists of two (R-Q) parallel circuits, which represent the contribution of the interfacial reaction and a passivating film. When fitting with this model, large errors occur in the low-frequency region and no significant variations of the different electrical-circuit element were found. Therefore, Models C and D are not suitable for this system either. When fitting with Model E, small errors occur in the low-frequency region.

The above six models were used to fit the impedance data obtained; it was found that the fitting results of model F are suitable to the actual passivation process. When fitting our theoretical electrical-equivalent circuit, a value of Chi-quadrate (χ^2) of approximately 10^{-4} was found and the fitting errors were quite small. Figure 7 shows, in all cases, that the correlation between experimental data and simulated data is very good.

The Bode plots and admittance plots (not shown) also displayed an acceptable agreement between experimental and simulated data, thereby validating the selected equivalent circuit model. Table 2 summarizes the values of the circuit parameters obtained from the best fit with the experimental impedance diagrams.

Same to charge-transfer resistance (R_{ct}), which does vary significantly with film formation potential, passive film resistance (R_P) varies with film formation potential. R_P increases considerably with film formation potential. This increase of R_P is accompanied by a decrease of Y_{0P} at every electrode potential, reflecting the growth and the thickening of the passive film or the decrease in the amount of charge carriers in the film [48]. One can notice the continuous decrease of R_P when the film formation potential increases and it highest value at films formed at 0.6 V. These results may be related to the presence and the competition of two kinds of oxides, chromium and iron. At low potentials (potentials lower than the transpassive potential of chromium), passive films are more enriched with chromium, making the films more protective [12]. At high potential in the passive range, chromium decreases continuously and iron increases progressively and hence the protective effect reduces [12, 48].

The values of the exponent n_2 obtained by fitting our EIS data were between 0.85 and 0.95, which points to a considerable passive film surface homogeneity; therefore, the constant phase element can be assumed to correspond to capacitive behavior while the values of n_1 and n_3 obtained can be associated with a distribution of the relaxation times as a result of heterogeneities present at the interfaces and static disorders such as porosity [48, 52].

The impedance of diffusion is independent of film formation potential. Defect transport is primarily due to migration under the influence of the electric field, and because the field strength is postulated to be independent

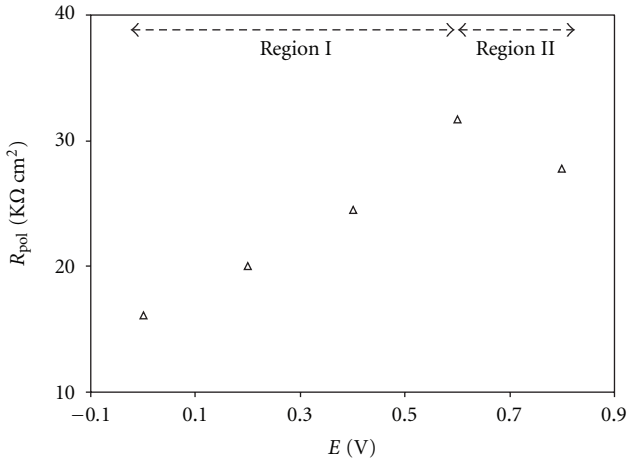

Figure 8: Effect of potential on polarization resistance of AISI 321 stainless steel in 0.5 M H_2SO_4.

of the applied potential in the point defect model, the impedance should be insensitive to the film formation potential [48, 53].

The variation of R_1 with the film formation potential is characteristic for uniform distribution of surface-states. The values of R_1 initially increased with film formation potential in the region I. At a sufficiently high potential ($E > 0.6$ V), which is close to the onset of the transpassive state, R_1 is observed to decrease with increasing formation potential [48].

The polarization resistance was taken to be the sum of R_1, R_P, R_D, and R_{ct}. Figure 8 shows the variation of polarization resistance with the film formation potential. The polarization resistance (R_{Pol}) initially increased with film formation potential in the region I. This is due to the establishment of the passive oxide layer. At a sufficiently high potential ($E > 0.6$ V), which is close to the onset of the transpassive state (Region II), the polarization resistance is observed to decrease with increasing potential. It has been reported that this is due to the oxidative ejection of Cr (VI) from the passive film [12].

4. Conclusion

The impedance data obtained for AISI 321 in sulphuric acid solution were adequately represented by an equivalent electrical circuit model based on PDM, comprising two $R//Q$ elements in series with a Z_D-$R//Q$ and an uncompensated solution resistance. The interfacial impedance and polarization resistance initially increased with applied potential. At a sufficiently high potential ($E > 0.6$ V), which is close to the initiation of the transpassive state, the interfacial impedance and polarization resistance were observed to decrease with increasing potential. The polarization resistance of AISI 321 stainless steel is of the order of 10^2 kΩ cm^2, commensurate with its high corrosion resistance.

References

[1] A. M. P. Simões, M. G. S. Ferreira, G. Lorang, and M. da Cunha Belo, "Influence of temperature on the properties of passive films formed on AISI 304 stainless steel," *Electrochimica Acta*, vol. 36, no. 2, pp. 315–320, 1991.

[2] S. Fujimoto, S. Kawachi, T. Nishio, and T. Shibata, "Impedance and photoelectrochemical properties of porous oxide film on Type304 stainless steel formed by square wave potential pulse polarization," *Journal of Electroanalytical Chemistry*, vol. 473, no. 1, pp. 265–271, 1999.

[3] E. Cho, S. Ahn, and H. Kwon, "Effects of EDTA on the electronic properties of passive film on Fe-20Cr in pH 8.5 buffer solution," *Electrochimica Acta*, vol. 50, no. 16-17, pp. 3383–3389, 2005.

[4] Z. Chen, C. Xu, N. Huang, X. Shi, S. Hu, and T. Zhang, "A study on the anodically passivated film of sus36 stainless steel," *Journal of Chinese Society for Corrosion and Protection*, vol. 11, no. 2, pp. 125–131, 1991.

[5] Y. S. Zhang, X. M. Zhu, M. Liu, and R. X. Che, "Effects of anodic passivation on the constitution, stability and resistance to corrosion of passive film formed on an Fe-24Mn-4Al-5Cr alloy," *Applied Surface Science*, vol. 222, no. 1–4, pp. 89–101, 2004.

[6] I. Olefjord, B. Brox, and U. Jelvestam, "Surface composition of stainless steels during anodic dissolution and passivation studied by ESCA," *Journal of the Electrochemical Society*, vol. 132, no. 12, pp. 2854–2861, 1985.

[7] J. E. Castle and J. H. Qiu, "A co-ordinated study of the passivation of alloy steels by plasma source mass spectrometry and x-ray photoelectron spectroscopy—1. Characterization of the passive film," *Corrosion Science*, vol. 29, no. 5, pp. 591–603, 1989.

[8] S. L. J. Gojkovic, S. K. Zecevic, and D. M. Drazic, "Oxygen reduction on iron—part VI. Processes in alkaline solutions," *Electrochimica Acta*, vol. 39, no. 7, pp. 975–982, 1994.

[9] R. Kirchheim, B. Heine, H. Fischmeister, S. Hofmann, H. Knote, and U. Stolz, "The passivity of iron-chromium alloys," *Corrosion Science*, vol. 29, no. 7, pp. 899–917, 1989.

[10] D. D. MacDonald, "The history of the point defect model for the passive state: a brief review of film growth aspects," *Electrochimica Acta*, vol. 56, no. 4, pp. 1761–1772, 2011.

[11] A. Fattah-alhosseini, M. A. Golozar, A. Saatchi, and K. Raeissi, "Effect of solution concentration on semiconducting properties of passive films formed on austenitic stainless steels," *Corrosion Science*, vol. 52, no. 1, pp. 205–209, 2010.

[12] A. Fattah-alhosseini, A. Saatchi, M. A. Golozar, and K. Raeissi, "The transpassive dissolution mechanism of 316L stainless steel," *Electrochimica Acta*, vol. 54, no. 13, pp. 3645–3650, 2009.

[13] A. Fattah-Alhosseini, A. Saatchi, M. A. Golozar, and K. Raeissi, "The passivity of AISI 316L stainless steel in 0.05 M HSO," *Journal of Applied Electrochemistry*, vol. 40, no. 2, pp. 457–461, 2010.

[14] D. D. Macdonald, "On the tenuous nature of passivity and its role in the isolation of HLNW," *Journal of Nuclear Materials*, vol. 379, no. 1–3, pp. 24–32, 2008.

[15] D. D. Macdonald and S. I. Smedley, "An electrochemical impedance analysis of passive films on nickel(111) in phosphate buffer solutions," *Electrochimica Acta*, vol. 35, no. 11-12, pp. 1949–1956, 1990.

[16] D. D. MacDonald, "On the existence of our metals-based civilization I. Phase-space analysis," *Journal of the Electrochemical Society*, vol. 153, no. 7, pp. B213–B224, 2006.

[17] D. D. Macdonald, K. M. Ismail, and E. Sikora, "Characterization of the passive state on zinc," *Journal of the Electrochemical Society*, vol. 145, no. 9, pp. 3141–3149, 1998.

[18] D. D. Macdonald, S. R. Biaggio, and H. Song, "Steady-state passive films. Interfacial kinetic effects and diagnostic criteria," *Journal of the Electrochemical Society*, vol. 139, no. 1, pp. 170–177, 1992.

[19] V. Horvat-Radošević, K. Kvastek, D. Hodko, and V. Pravdić, "Impedance of anodically passivated FeB over potentials from passive state to oxygen evolution," *Electrochimica Acta*, vol. 39, no. 1, pp. 119–130, 1994.

[20] J. M. Blengino, M. Keddam, J. P. Labbe, and L. Robbiola, "Physico-chemical characterization of corrosion layers formed on iron in a sodium carbonate-bicarbonate containing environment," *Corrosion Science*, vol. 37, no. 4, pp. 621–643, 1995.

[21] E. B. Castro and J. R. Vilche, "Investigation of passive layers on iron and iron-chromium alloys by electrochemical impedance spectroscopy," *Electrochimica Acta*, vol. 38, no. 11, pp. 1567–1572, 1993.

[22] M. Gaberšček and S. Pejovnik, "Impedance spectroscopy as a technique for studying the spontaneous passivation of metals in electrolytes," *Electrochimica Acta*, vol. 41, no. 7-8, pp. 1137–1142, 1996.

[23] J. A. Bardwell, G. I. Sproule, B. MacDougall, M. J. Graham, A. J. Davenport, and H. S. Isaacs, "In situ XANES detection of Cr(VI) in the passive film on Fe-26Cr," *Journal of the Electrochemical Society*, vol. 139, no. 2, pp. 371–373, 1992.

[24] S. Ningshen, U. K. Mudali, G. Amarendra, P. Gopalan, R. K. Dayal, and H. S. Khatak, "Hydrogen effects on the passive film formation and pitting susceptibility of nitrogen containing type 316L stainless steels," *Corrosion Science*, vol. 48, no. 5, pp. 1106–1121, 2006.

[25] D. Wallinder, J. Pan, C. Leygraf, and A. Delblanc-Bauer, "EIS and XPS study of surface modification of 316LVM stainless steel after passivation," *Corrosion Science*, vol. 41, no. 2, pp. 275–289, 1998.

[26] H. H. Ge, G. D. Zhou, and W. Q. Wu, "Passivation model of 316 stainless steel in simulated cooling water and the effect of sulfide on the passive film," *Applied Surface Science*, vol. 211, no. 1–4, pp. 321–334, 2003.

[27] M. A. Ameer, A. M. Fekry, and F. E. T. Heakal, "Electrochemical behaviour of passive films on molybdenum-containing austenitic stainless steels in aqueous solutions," *Electrochimica Acta*, vol. 50, no. 1, pp. 43–49, 2004.

[28] A. Pardo, M. C. Merino, M. Carboneras, F. Viejo, R. Arrabal, and J. Muñoz, "Influence of Cu and Sn content in the corrosion of AISI 304 and 316 stainless steels in HSO," *Corrosion Science*, vol. 48, no. 5, pp. 1075–1092, 2006.

[29] C. A. Huang, Y. Z. Chang, and S. C. Chen, "The electrochemical behavior of austenitic stainless steel with different degrees of sensitization in the transpassive potential region in 1 M HSO containing chloride," *Corrosion Science*, vol. 46, no. 6, pp. 1501–1513, 2004.

[30] A. M. Schmidt, D. S. Azambuja, and E. M. A. Martini, "Semiconductive properties of titanium anodic oxide films in McIlvaine buffer solution," *Corrosion Science*, vol. 48, no. 10, pp. 2901–2912, 2006.

[31] W. Ye, Y. Li, and F. Wang, "Effects of nanocrystallization on the corrosion behavior of 309 stainless steel," *Electrochimica Acta*, vol. 51, no. 21, pp. 4426–4432, 2006.

[32] F. El-Taib Heakal, A. A. Ghoneim, and A. M. Fekry, "Stability of spontaneous passive films on high strength Mo-containing stainless steels in aqueous solutions," *Journal of Applied Electrochemistry*, vol. 37, no. 3, pp. 405–413, 2007.

[33] F. J. Martin, G. T. Cheek, W. E. O'Grady, and P. M. Natishan, "Impedance studies of the passive film on aluminium," *Corrosion Science*, vol. 47, no. 12, pp. 3187–3201, 2005.

[34] M. E. Orazem and B. Tribollet, *Electrochemical Impedance Spectroscopy*, John Wiley & Sons, Hoboken, NJ, USA, 2008.

[35] E. M. A. Martini and I. L. Muller, "Characterization of the film formed on iron borate solution by electrochemical impedance spectroscopy," *Corrosion Science*, vol. 42, no. 3, pp. 443–454, 2000.

[36] Y. X. Qiao, Y. G. Zheng, W. Ke, and P. C. Okafor, "Electrochemical behaviour of high nitrogen stainless steel in acidic solutions," *Corrosion Science*, vol. 51, no. 5, pp. 979–986, 2009.

[37] F. El-Taib Heakal, A. A. Ghoneim, and A. M. Fekry, "Stability of spontaneous passive films on high strength Mo-containing stainless steels in aqueous solutions," *Journal of Applied Electrochemistry*, vol. 37, no. 3, pp. 405–413, 2007.

[38] H. Ma, X. Cheng, G. Li et al., "The influence of hydrogen sulfide on corrosion of iron under different conditions," *Corrosion Science*, vol. 42, pp. 1669–1683, 2000.

[39] C. Y. Chao, L. F. Lin, and D. D. Macdonald, "Point defect model for anodic passive films," *Journal of Non-Crystalline Solids*, vol. 353, pp. 1874–1879, 2007.

[40] T. Hong, M. Nagumo, and W. P. Jepson, "Influence of HNO_3 treatments on the early stages of pitting of type 430 stainless steel," *Corrosion Science*, vol. 42, no. 2, pp. 289–298, 2000.

[41] J.-B. Lee, "Effects of alloying elements, Cr, Mo and N on repassivation characteristics of stainless steels using the abrading electrode technique," *Materials Chemistry and Physics*, vol. 99, no. 2-3, pp. 224–234, 2006.

[42] M. Sánchez, J. Gregori, C. Alonso, J. J. García-Jareño, H. Takenouti, and F. Vicente, "Electrochemical impedance spectroscopy for studying passive layers on steel rebars immersed in alkaline solutions simulating concrete pores," *Electrochimica Acta*, vol. 52, no. 27, pp. 7634–7641, 2007.

[43] M. Sánchez, J. Gregori, M. C. Alonso, J. J. García-Jareño, and F. Vicente, "Anodic growth of passive layers on steel rebars in an alkaline medium simulating the concrete pores," *Electrochimica Acta*, vol. 52, no. 1, pp. 47–53, 2006.

[44] Z. F. Yin, W. Z. Zhao, W. Y. Lai, and X. H. Zhao, "Electrochemical behaviour of Ni-base alloys exposed under oil/gas field environments," *Corrosion Science*, vol. 51, no. 8, pp. 1702–1706, 2009.

[45] J. Jamnik, J. Maier, and S. Pejovnik, "Powerful electrical network model for the impedance of mixed conductors," *Electrochimica Acta*, vol. 44, no. 24, pp. 4139–4145, 1999.

[46] N. Priyantha, P. Jayaweera, D. D. Macdonald, and A. Sun, "An electrochemical impedance study of alloy 22 in NaCl brine at elevated temperature. I. Corrosion behavior," *Journal of Electroanalytical Chemistry*, vol. 572, no. 2, pp. 409–419, 2004.

[47] B. D. Cahan and C. T. Chen, "Nature of the passive film on iron—3. The chemi-conductor model and further supporting evidence," *Journal of the Electrochemical Society*, vol. 129, no. 5, pp. 921–925, 1982.

[48] L. Hamadou, A. Kadri, N. Benbrahim, and J. P. Petit, "Characterization of thin anodically grown oxide films on AISI 304L stainless steel," *Journal of the Electrochemical Society*, vol. 154, no. 12, pp. G291–G297, 2007.

[49] B. Beverskog, M. Bojinov, P. Kinnunen, T. Laitinen, K. Mäkelä, and T. Saario, "A mixed-conduction model for oxide films on Fe, Cr and Fe-Cr alloys in high-temperature aqueous electrolytes—II. Adaptation and justification of the model," *Corrosion Science*, vol. 44, no. 9, pp. 1923–1940, 2002.

[50] M. Bojinov, P. Kinnunen, K. Lundgren, and G. Wikmark, "A mixed-conduction model for the oxidation of stainless steel in a high-temperature electrolyte estimation of kinetic parameters of oxide layer growth and restructuring," *Journal of the Electrochemical Society*, vol. 152, no. 7, pp. B250–B261, 2005.

[51] M. Bojinov, G. Fabricius, P. Kinnunen et al., "Electrochemical study of the passive behaviour of Ni-Cr alloys in a borate solution—a mixed-conduction model approach," *Journal of Electroanalytical Chemistry*, vol. 504, no. 1, pp. 29–44, 2001.

[52] D. Qu, "Application of a.c. impedance technique to the study of the proton diffusion process in the porous MnO electrode," *Electrochimica Acta*, vol. 48, no. 12, pp. 1675–1684, 2003.

[53] E. Sikora and D. D. Macdonald, "Nature of the passive film on nickel," *Electrochimica Acta*, vol. 48, no. 1, pp. 69–77, 2002.